DESIGN OF A CARBON FIBER REINFORCED PLASTIC SHAFT FOR A HIGH SPEED FLYWHEEL ROTOR

Stefan Hartl, Alexander Schulz and Manfred Kaltenbacher

Institute of Mechanics and Mechatronics, Vienna University of Technology
Getreidemarkt 9 (BA06), 1060 Vienna, Austria
Email: stefan.hartl@tuwien.ac.at, web page: http://www.mec.tuwien.ac.at

Keywords: Flywheel energy storage system, Finite element analysis, Carbon fiber reinforced polymer, Modal analysis, Genetic algorithm

ABSTRACT

This paper discusses a new flywheel rotor design, containing a carbon fiber reinforced polymer (CFRP) hollow shaft with different winding angles and a hoop wound inertia mass with rectangular cross section, computed using a bending natural frequency and strength safety factor optimization. The input specifications for optimization are a minimum useable energy of 5kWh, a given rotor geometry and minimum stress safety factor. The optimization is performed using a genetic algorithm. The rotordynamic finite element (FE) model of the flywheel rotor is used as fitness function and a static FE model of the rotor serves the nonlinear constraint function. The hollow shaft and the inertia mass are designed of high strength and high modulus CFRP. The material parameters of the used CFRP material are measured by several tensile tests and the specimen and the hollow shaft are manufactured by filament winding followed by CNC machining. The simulation of the flywheel rotor shaft is then validated by modal analysis using a laser scanning vibrometer.

1 INTRODUCTION

Flywheel energy storage systems (FESS) represent an ecologically and economically sustainable technology for decentralized energy storage. Long life cycles without performance degradation depending on depth of discharge (DoD) and a minimum of systematic maintenance are key advantages of this technology. Within the nationally supported research project ``Long Term Storage Flywheel``, ``Optimum Shape Flywheel`` and in cooperation with the company FWT Composites & Rolls GmbH, a FESS utilizing highest achievable energy density along with the required manufacturing technology is developed. To achieve high energy densities, the rotor of FESS are usually manufactured of fiber reinforced plastics (FRP) by the filament winding process. Carbon fiber reinforced plastics (CFRP) show a high specific strength compared to other materials and are therefore often used as material for the inertia mass.

Accurate prediction of the natural frequencies and mode shapes of the rotor are necessary to prevent excessive bearing loss and even catastrophic failure [1]. The finite element (FE) method is used to calculate the change in natural frequencies by rotordynamic analysis and to perform stress analysis at maximum rotor speed. Common innrunner - FESS consist of magnetic bearings, motor components and inertia mass that are mounted on a metal shaft, typically aluminum or steel, due to the well known material parameters, easy manufacturing and low costs. The complex construction of such rotors lead to some modeling effort. The modeling of the ferro-magnetic laminated core of motor components is studied in [2]. A large overview of serveral influencing factors, e.g. bearing stiffness and damping, support stiffness, rotor stiffness and rotor weight, on the modal characteristics and critical speeds is summarized in [3]. The rotordynamic analysis in [4] shows the modeling of a composite rotor made of orthotropic material including material damping.

This paper presents in the first part the rotordynamic modeling, stress analysis and optimization of a CFRP hollow shaft used in a 5kWh FESS as shown in Fig. 1. The second part contains the manufacturing of the shaft, followed by the measurement of the natural frequencies and mode shapes using a laser scanning vibrometer.

a) 

b) 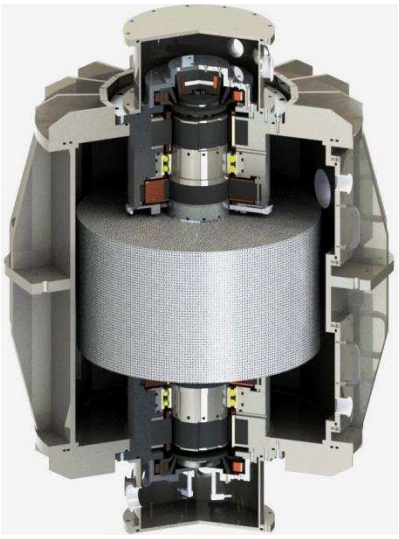

Figure 1: 5kWh flywheel energy storage system: (a) test rig; (b) schematic view of the rotor and containment.

2 MATERIALS AND MODELS

2.1 Material parameter identification

The used CFRP specimens (hoop wound pipes and unidirectional plates) were manufactured by FWT Composites & Rolls GmbH using high strength fabric 24 K T800H roving and epoxy resin. A fully automated CNC filament winding machine was used for the specimen production. The fibre tension during winding was kept constant at 20 N. The wet band of 6 mm width, were wound over a steel mandrel (cylinder and rectangular cross section) followed by curing in two different steps: 2 h at 80°C followed by 6 h at 160°C. The samples were then cut out according to the final sample geometry. All the samples were then quality checked and some of them additionally outfitted with strain gauges. For tensile testing at the Institute of Materials Science and Technology (Vienna University of Technology), a Zwick Z250 Universal Testing System with a load capacity of 250 kN was used. During the tensile test the loading rate of the testing machine was kept constant at a level of 2 mm/min and the load and strain data were measured until failure of the specimen. Table 1 summarizes the measured material parameters and other material parameters used for simulation.

2.2 Material modeling

The aluminum, steel and ferro-magnetic sections are modeled by isotropic mechanical behaviour. The hollow shaft is separated into three cylinders with different but constant positive and negative winding angle α_i. Hence, the cylinders can be obtained by several plies of embedded fibers and so each ply has an orthotropic mechanical behaviour, as shown in Fig. 2.

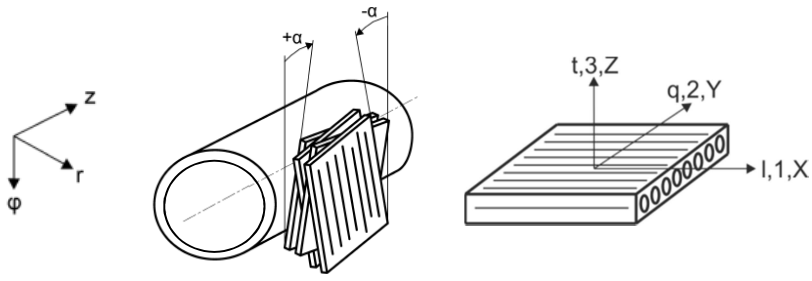

Figure 2: Composite cylinder and plan of ply.

Properties		T800H/epoxy 60% vol.	K13916/epoxy 60% vol.	Steel	Aluminum	Ferro-magnetic
E_1	[GPa]	140	290	210	70	210
E_2	[GPa]	7.8	7.8	210	70	210
E_3	[GPa]	7.8	7.8	210	70	210
$\nu_{12}=\nu_{13}$	–	0.4	0.4	0.3	0.3	0.3
ν_{23}	–	0.38	0.38	0.3	0.3	0.3
$G_{12}=G_{13}$	[GPa]	3.4	3.9	80.7	26.9	80.7
P	[kg/m³]	1617	1815	7850	2700	8150
X_t	[MPa]	2200	1300	–	–	–
X_c	[MPa]	1000	470	–	–	–
$Y_t= Z_t$	[MPa]	24	19	–	–	–
$Y_c= Z_c$	[MPa]	113	105	–	–	–
$S_{12}=S_{13}$	[MPa]	57	25	–	–	–
S_{23}	[MPa]	14	14	–	–	–
V. mises	[MPa]	–	–	800	450	600

Table 1: Material parameter

The generalized Hooke's law for an orthotropic material in the local ply l, q, t-frame reads as

$$\underbrace{\begin{bmatrix}\sigma_{ll}\\ \sigma_{qq}\\ \sigma_{tt}\\ \tau_{lq}\\ \tau_{lt}\\ \tau_{qt}\end{bmatrix}}_{\boldsymbol{\sigma}_l} = \underbrace{\begin{bmatrix} E_{ll} & E_{lq} & E_{lt} & 0 & 0 & 0\\ & E_{qq} & E_{qt} & 0 & 0 & 0\\ & & E_{tt} & 0 & 0 & 0\\ & & & G_{lq} & 0 & 0\\ & sym. & & & G_{lt} & 0\\ & & & & & G_{qt}\end{bmatrix}}_{\boldsymbol{E}_l} \cdot \underbrace{\begin{bmatrix}\varepsilon_{ll}\\ \varepsilon_{qq}\\ \varepsilon_{tt}\\ \gamma_{lq}\\ \gamma_{lt}\\ \gamma_{qt}\end{bmatrix}}_{\boldsymbol{\varepsilon}_l}, \tag{1}$$

where $\boldsymbol{\sigma}_l$ and $\boldsymbol{\epsilon}_l$ are the stress and strain fields, $\boldsymbol{E}_l$ is the material stiffness tensor and its components are computed by the following relations

$$\begin{aligned} \Delta &= \frac{1-2\nu_{12}\nu_{21}-2\nu_{21}\nu_{23}\nu_{12}-\nu_{23}^2}{E_1E_2^2},\\ G_{qt} &= \frac{E_2}{2(1+\nu_{23})}, \qquad \frac{\nu_{ij}}{E_i} = \frac{\nu_{ji}}{E_j},\ \ i,j=1,2,3\,,\\ E_{ll} &= \frac{1-\nu_{23}^2}{E_2^2\Delta}, \qquad E_{lq} = \frac{\nu_{21}+\nu_{21}\nu_{23}}{E_2^2\Delta},\\ E_{qq} &= \frac{1-\nu_{12}\nu_{21}}{E_1E_2\Delta}, \qquad E_{qt} = \frac{\nu_{23}+\nu_{12}\nu_{21}}{E_1E_2\Delta},\\ E_{tt} &= \frac{1-\nu_{12}\nu_{21}}{E_1E_2\Delta}, \qquad E_{lt} = \frac{\nu_{21}+\nu_{21}\nu_{23}}{E_2^2\Delta}. \end{aligned} \tag{2}$$

The overall mechanical behaviour in the global frame (r, φ, z) can be described by transformation of the local stiffness tensor $\boldsymbol{E}_l$. Due to the positive and negative winding angle and the assumption of an even number of plies in each section, the global stiffness tensor $\boldsymbol{E}_g$ computes as

$$\boldsymbol{E}_g = \frac{1}{2}\left[\boldsymbol{T}(\alpha)^{-1}\boldsymbol{E}_l\,\boldsymbol{T}(\alpha)^{-1^T} + \boldsymbol{T}(-\alpha)^{-1}\boldsymbol{E}_l\,\boldsymbol{T}(-\alpha)^{-1^T}\right] \tag{3}$$

using the transfer matrix $\boldsymbol{T}$ with $c = \cos(\alpha)$ and $s = \sin(\alpha)$ given by

$$\boldsymbol{T}(\alpha) = \begin{bmatrix} c^2 & s^2 & 0 & 0 & 0 & 2cs \\ s^2 & c^2 & 0 & 0 & 0 & -2cs \\ 0 & 0 & 1 & 0 & 0 & 0 \\ 0 & 0 & 0 & c & -s & 0 \\ 0 & 0 & 0 & s & c & 0 \\ -cs & cs & 0 & 0 & 0 & c^2 - s^2 \end{bmatrix}. \tag{4}$$

2.3 Rotordynamic modeling

For modal analysis of the FESS rotor, the FE modeling software ANSYS 13.0 ([5]) was used with pre-stressing of the rotating structure using the following semi-discrete Galerkin formulation for structural mechanics in the stationary frame:

$$\boldsymbol{M} \cdot \ddot{\boldsymbol{U}} + (\boldsymbol{G} + \boldsymbol{C}) \cdot \dot{\boldsymbol{U}} + (\boldsymbol{B} + \boldsymbol{K}) \cdot \boldsymbol{U} = \boldsymbol{f}\,, \tag{5}$$

where $\boldsymbol{M}$, $\boldsymbol{G}$, $\boldsymbol{C}$, $\boldsymbol{B}$, $\boldsymbol{K}$ and $\boldsymbol{f}$ denotes the mass, gyroscopic, damping, rotating damping and stiffness matrix, and $\boldsymbol{f}$ is the external force vector. The rotordynamic model consists of areas representing the components of the rotor, as displayed in Fig. 3. Each area is meshed using SOLID273 generalized axisymmetric solid 8 node elements to perform a full 3D analysis with minimal simulation effort. The characteristic of the magnetic bearing was simplified using the COMBI214 2D stiffness and damping element at the location of the radial bearings. For all simulation the material parameters as listed in Table 1, are used. Additional parameters are given in Table 2. From the minimal achievable stored energy and the given rotor geometry, the maximum speed of rotation was used to set up the Campbell diagram. In total, five incremental steps were used to calculate the Campbell diagram to find the critical speeds.

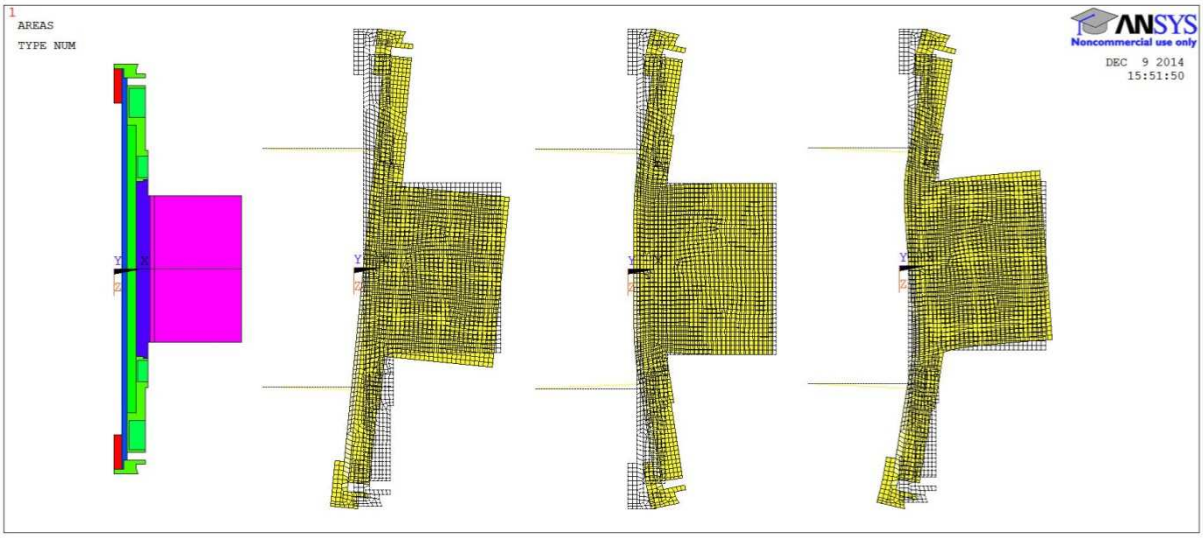

Figure 3: Rotordynamic analysis, defined areas and resulting sample mode shapes.

Max. speed	[rpm]	10000
Max. element size	[mm]	5
Bearing stiffness [6]	[N/m]	50000
Bearing damping [6]	[Ns/m]	320

Table 2: Parameters for calculation

2.4 Stress analysis

For stress analysis, the rotor model was built up in the FE software COMSOL MULTIPHYSICS 4.2a ([7]) to perform a quasi-static analysis with press fit between the inertia mass and the hollow shaft. The axisymmetric model of the rotor, as can be seen in Fig. 4, was discretized by quadrilateral finite elements and by using the rφ-symmetry plane. For the CFRP rotor and the shaft components the material parameters are listed in Table 1. The stress state of this FESS rotor was calculated in two steps. In a first step the thermal shrink fit of the shaft onto the inertia mass and in a second step the inertial loads due to rotation was computed. The global stress state was transformed back into the local frame and then the generalized quadratic Tsai-Wu criterion [8] was considered to perform the failure estimation

$$\overline{\boldsymbol{F}}^T \boldsymbol{\sigma}_l + \boldsymbol{\sigma}_l^T \widetilde{\boldsymbol{F}} \boldsymbol{\sigma}_l = 1 \, . \tag{6}$$

The local stress state vector $\boldsymbol{\sigma}_l$ and $\overline{\boldsymbol{F}}$, $\widetilde{\boldsymbol{F}}$ the second and fourth order tensor of the strength parameters compute by

$$\overline{\boldsymbol{F}} = \begin{bmatrix} F_1 \\ F_2 \\ F_3 \\ 0 \\ 0 \\ 0 \end{bmatrix}, \quad \widetilde{\boldsymbol{F}} = \begin{bmatrix} F_{11} & F_{12} & F_{13} & 0 & 0 & 0 \\ & F_{22} & F_{23} & 0 & 0 & 0 \\ & & F_{33} & 0 & 0 & 0 \\ & & & F_{44} & 0 & 0 \\ & & & & F_{55} & 0 \\ sym. & & & & & F_{66} \end{bmatrix},$$

$$\begin{aligned} F_1 &= \frac{1}{X_t} - \frac{1}{X_c}, & F_2 &= \frac{1}{Y_t} - \frac{1}{Y_c}, \\ F_3 &= \frac{1}{Z_t} - \frac{1}{Z_c}, & F_{11} &= \frac{1}{X_t X_c}, \\ F_{22} &= \frac{1}{Y_t Y_c}, & F_{33} &= \frac{1}{Z_t Z_c}, \\ F_{44} &= \frac{1}{S_{23}^2}, & F_{55} &= \frac{1}{S_{13}^2}, \\ F_{66} &= \frac{1}{S_{12}^2}, & F_{12} &= -\frac{1}{2}\sqrt{F_{11}F_{22}}, \\ F_{13} &= -\frac{1}{2}\sqrt{F_{11}F_{33}}, & F_{23} &= -\frac{1}{2}\sqrt{F_{33}F_{22}}. \end{aligned} \tag{7}$$

.

Thereby, the values listed in Table 1 have been used. The safety factor $S_{R_{TW}}$ is introduced as a proportional factor as follows

$$\mathrm{S}_{R_{TW}} = \frac{1}{R_{TW}} = \frac{\sigma^*}{\sigma} \, . \tag{8}$$

Thereby, $1/R_{TW}$ links the actual stress state $\boldsymbol{\sigma}$ and the stress state $\boldsymbol{\sigma}^*$ that causes material failure. Combining Eqs. (6) and (8) and defining $\boldsymbol{\sigma} = \boldsymbol{\sigma}^*$ results in a quadratic equation with the following (positive) solution for the safety factor

$$\frac{1}{R_{TW}} = \frac{-\overline{\boldsymbol{F}}^T \boldsymbol{\sigma}_l + \sqrt{(\overline{\boldsymbol{F}}^T \boldsymbol{\sigma}_l)^2 + 4\boldsymbol{\sigma}_l^T \widetilde{\boldsymbol{F}} \boldsymbol{\sigma}_l}}{2\boldsymbol{\sigma}_l^T \widetilde{\boldsymbol{F}} \boldsymbol{\sigma}_l}. \tag{8}$$

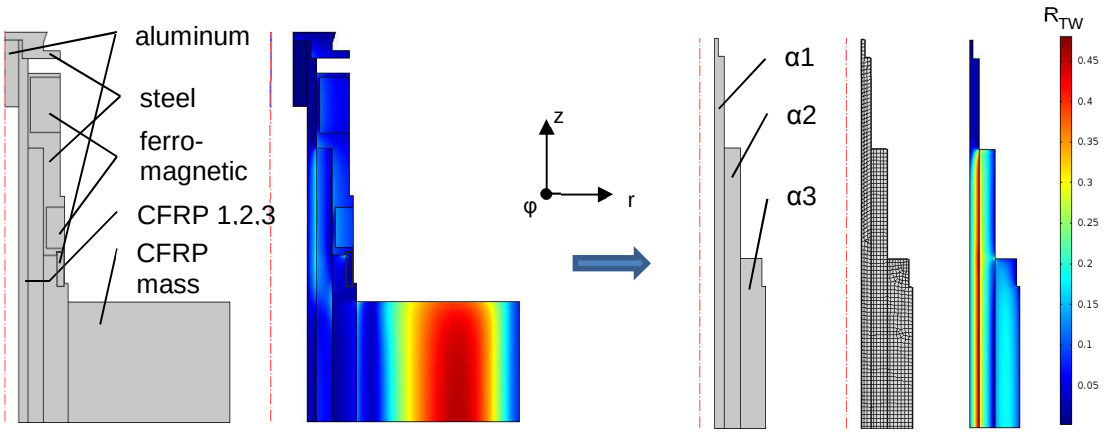

Figure 4: Stress analysis, defined sections and model simplification.

2.5 Optimization using genetic algorithm

The optimization was performed using a genetic algorithm implemented in MATLAB R2010b. The optimality problem is to construct a FE model by use of three design variables – the winding angles of the three different sections: $\boldsymbol{\alpha_1}$, $\boldsymbol{\alpha_2}$ and $\boldsymbol{\alpha_3}$ – and an objective function using a constraint function. The rotordynamic FE model of the FESS rotor is used as fitness function to evaluate the natural frequencies. A simplified static FE model, shown in Fig. 4, of the rotor gives the nonlinear constraint function. The static model was simplified to reduce simulation effort. Another constraint is the maximum allowable winding angle of about 70° to guarantee a possible manufacturing of the hollow shaft and a step size of 1° is used. The objective function as well as the constraints is shown in Fig 5. The goal of the optimization is to find the winding angle triple which maximizes the minimum of the first and the second bending natural frequency for the given input of geometry, safety factor $\boldsymbol{S_{R_{TW}} = 2}$ for stress analysis and a minimum energy content $\boldsymbol{E_{min} = 1.37}$ kWh. By fulfilling the nonlinear constraint function a maximum rotating speed can be calculated that leads to maximum energy content, and with the Campbell diagram a safety factor $\boldsymbol{S_{fB}}$ against reaching the lowest bending natural frequency due to the optimal solution for the winding angles can be found.

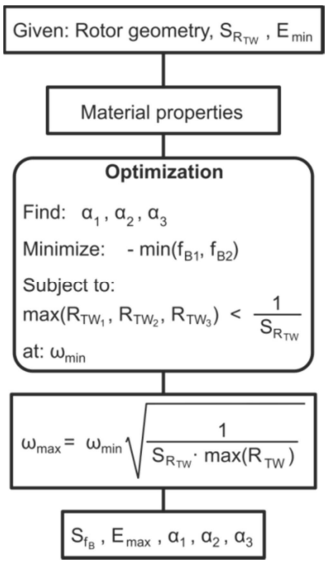

Figure 5: Optimization scheme.

3 RESULTS AND DISCUSSION

In this section the results of the optimization of the FESS rotor is described, followed by the fabrication of the hollow CFRP shaft and assembling of the rotor shaft. The rotor shaft without inertia mass has then been analysed using modal analysis to validate the simulation in the zero rotating speed case.

3.1 Optimal solution for winding angles

A population size of 200 and ten elite individuals after 45 generations resulted in a winding angle optimum combination of $\alpha_1 = 19°$, $\alpha_2 = 69°$ and $\alpha_3 = 13°$ for a rotational speed of 10000 rpm. This leads to a natural frequency of 379 Hz for the first U-shaped bending mode at this speed. The stress analysis at this speed results in a safety factor of $S_{R_{TW}} = 2{,}56$. Hence, the speed can be increased to 10800 rpm until failure in the hollow shaft occurs. For this case the Campbell diagram has to be enlarged and it can be found that the overall critical speed is 22700 rpm until the first forward mode is reached. The safety factor against reaching the first bending natural frequency is $S_{fB} = 2{,}1$, as can be seen in Fig. 6. The mode shapes of the 1st and 2nd bending mode are depicted in Fig. 7.

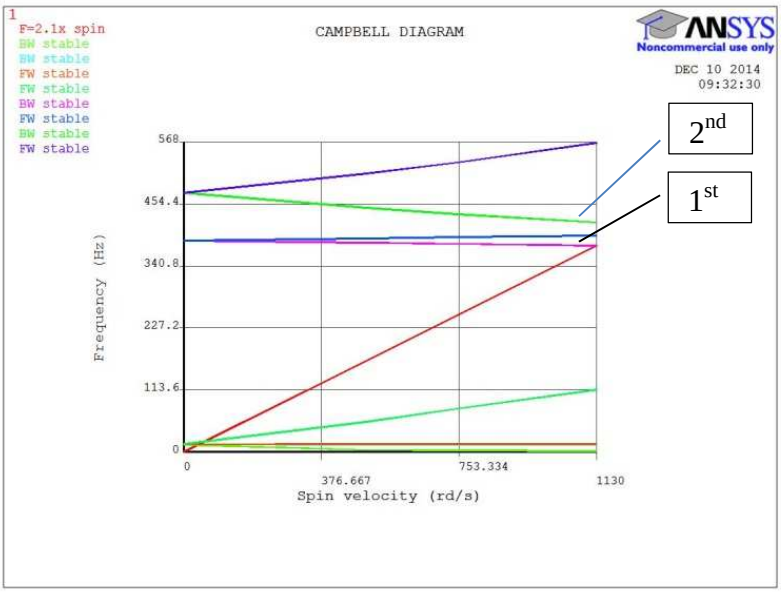

Figure 6: Campbell diagram of FESS rotor: tilt mode, 1st and 2nd bending mode and critical speed.

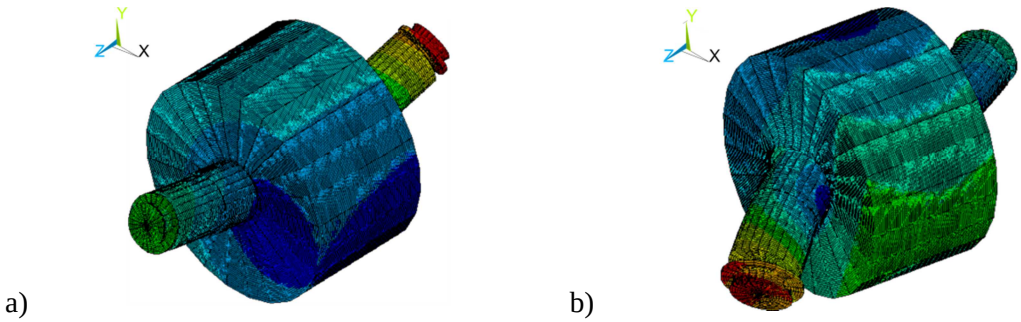

a) b)

Figure 7: Bending mode shapes: (a) 1st mode ‘U-shape’ at 379 Hz; (b) 2nd mode ’S-shape’ at 425 Hz.

a) 

b) 

c) 

Figure 8: CFRP hollow shaft: (a) mandrel with symmetric mounted winding-pins; (b) winding of the hollow shaft; (c) finished machined shaft.

3.2 Fabrication of the CFRP hollow shaft

The hollow shaft was manufactured using filament winding process by FWT Composites & Rolls GmbH. In total, a set of six 24 K rovings was combined to achieve a band thickness of about 19 mm. The different winding angels were applied using different rotating and translational speeds of the CNC winding machine. The sections including the lowest winding angles were manufactured using special winding-pins that were mounted on the mandrel before winding operation to guarantee a slight pretension force (see Fig. 8).

3.3 Modal characteristics (from experimental data)

Vibration modal analysis is performed on the shaft by laser scanning vibrometer. Therefor, the shaft was supported by free-free boundary conditions and was excited with a shaker using frequency limited white noise (0-2 kHz) (see Fig. 9). The movement of the axis was observed in 129 points. Then the first three natural bending frequencies and the corresponding mode shapes were extracted. The average values of the natural frequencies are listed in Table 3 and the measured mode shapes are depicted in Fig. 10.

Mode shape	'U' shaped	'S' shaped	'M' shaped
Experiment	368	874	1291
FE model	399	868	1204

Table 3: Experimental and modeled natural frequencies (Hz).

a)

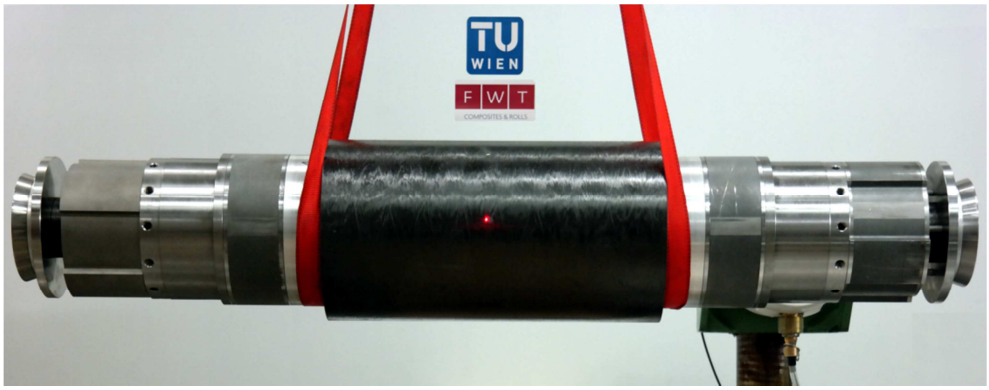

b)

Figure 9: Modal analysis of the shaft: (a) free-free support; (b) force excitation by shaker.

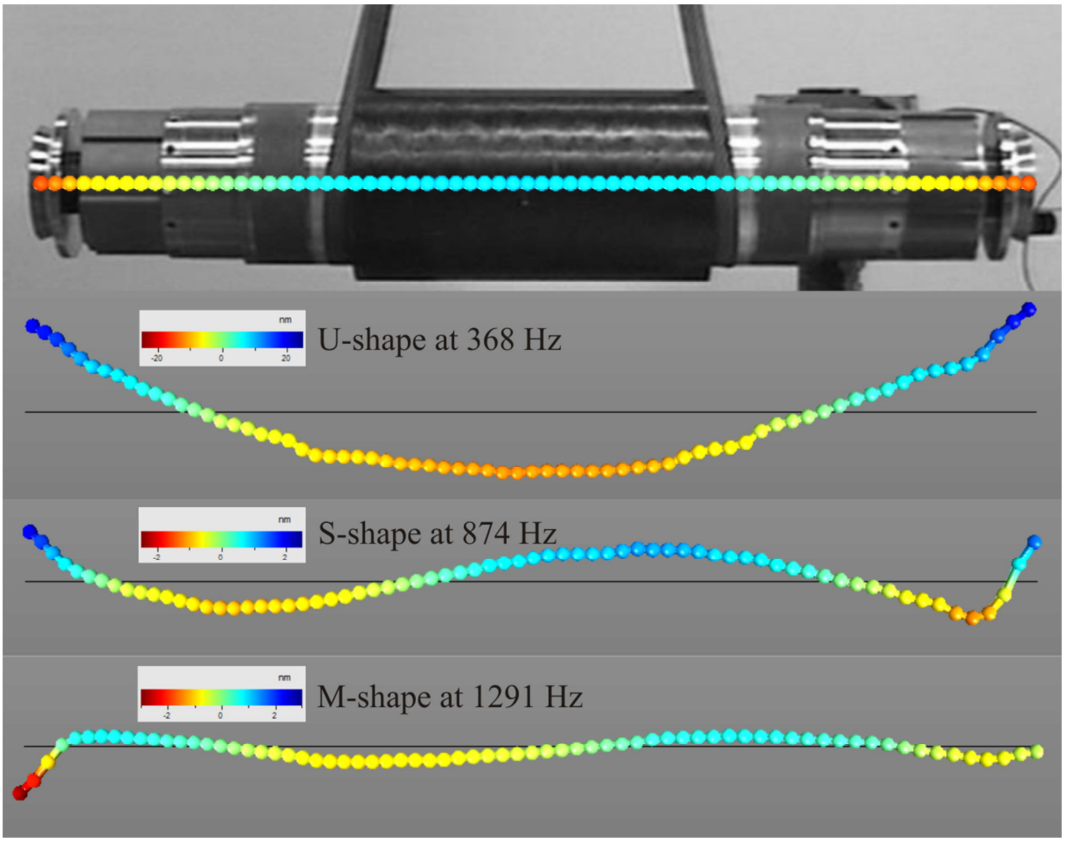

Figure 10: Measured mode shapes, out of plane deformation (nm).

3.3 Modal characteristics (from FE analysis)

The bending natural frequencies for the FE model of the shaft are also computed with the absence of the inertia mass and then compared to the experimental data. The results listed in Table 3 clearly demonstrate that the shaft natural frequencies of the FE model agree well with those obtained by modal analysis. The first three mode shapes are depicted in Fig 11.

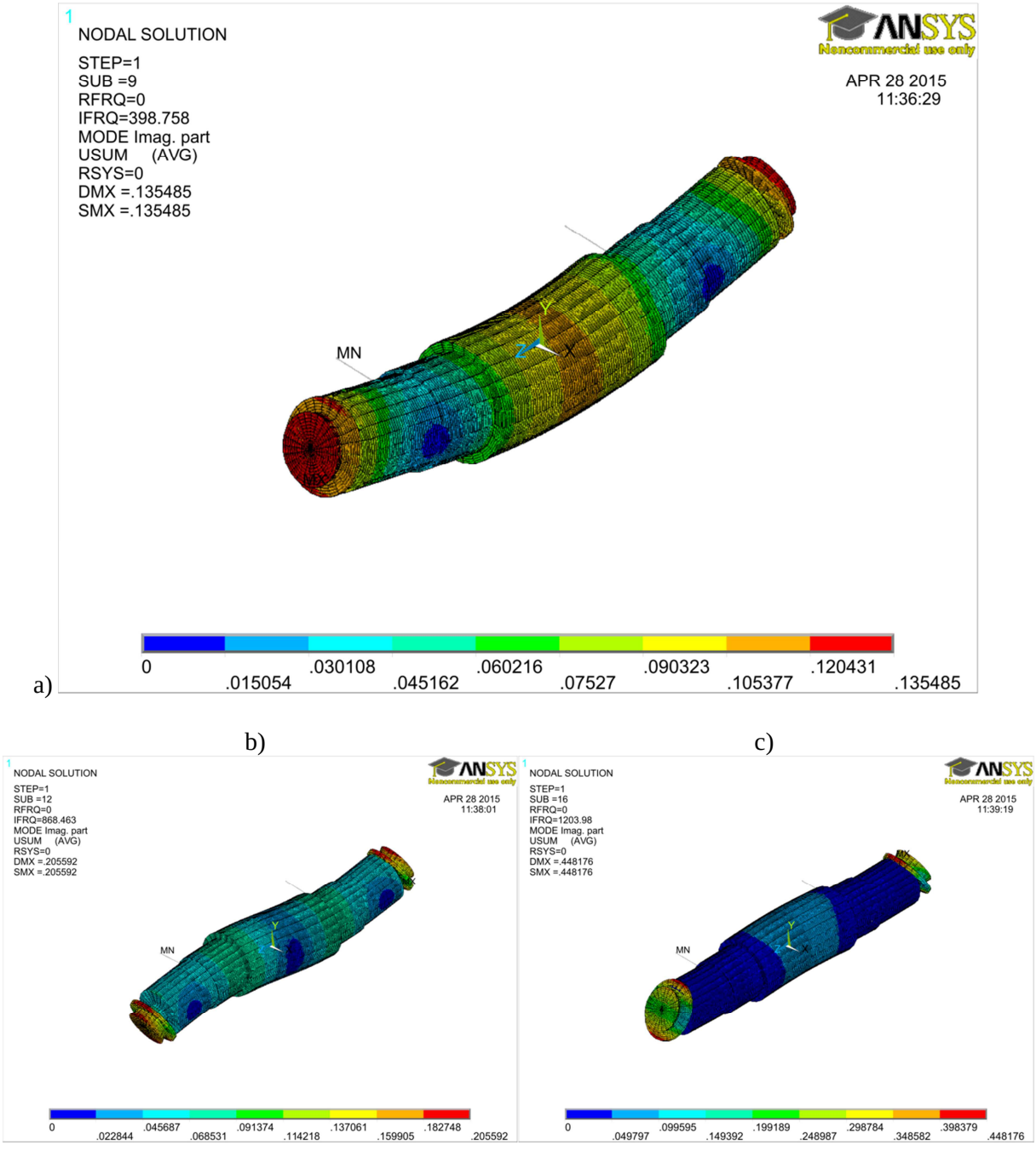

Figure 11: FE mode shapes of the shaft for the static case: (a) 1st mode ‘U-shape’ at 399 Hz; (b) 2nd mode ’S-shape’ at 872 Hz; (c) 3rd mode ’M-shape’ at 1204 Hz.

4 CONCLUSION

In this paper an optimization of a CFRP hollow shaft with different winding angles as design variables is presented. The fitness and nonlinear constraint function are given by a rotordynamic and static stress FE analysis to calculate the lowest natural bending frequency and to perform failure prediction of the CFRP material due to rotating speed. To identify the parameters of the used CFRP-material, a set of tensile tests has been carried out. The CFRP hollow shaft was then manufactured and the bearing and motor components were assembled followed by a modal analysis to measure the natural frequencies and mode shapes. This was carried out by using a laser scanning vibrometer and a shaker for excitation using band limited white noise. The experimental analysis compares well to the rotordynamic simulation for zero rotating speed as a first measuring result. Further measurements will be carried out with the press-fitted inertia mass at operating conditions using the presented flywheel test rig. Furthermore, due to the hollow shaft, a wireless measurement system will be included in the hollow shaft to observe the stress and bending movement of the rotor during rotation.

ACKNOWLEDGEMENT

The presented work is part of the research project “Optimum Shape Flywheel” and is supported by “Klima- und Energiefonds” in line with the program “NEUE ENERGIEN 2020” conducted by the Austrian Research Agency (FFG).

REFERENCES

[1] B. Bai, L. Zhang, T. Guo and C. Liu, Analysis of dynamic characteristics of the main shaft system in a hydro-turbine Based on ANSYS, *Procedia Engineering*, **31**, 2012, pp. 654-658.

[2] S. Singhal, K.V. Singh and A. Hyder, Effect of laminated core on rotor mode shape of large high speed induction motor, *Proceedings of the International Electric Machines & Drives Conference, Niagara Falls, ON, Canada, 2011*.

[3] R. Mistry, B. Finley, S. Kreitzer and R. Queen, Influencing factors on motor vibration & rotor critical speed in design, test and field applications, *Proceedings of the International Petroleum and Chemical Industry Technical Conference, San Francisco, CA, USA, 2014.*

[4] R. Sino, T.N. Baranger, E. Chatelet, and G. Jacquet, Dynamic analysis of a rotating composite shaft, *Composites Science and Technology*, **68**, 2008, pp. 337-345.

[5] ANSYS® Academic Research, Release 13.0, Help System, *Rotordynamic Analysis Guide, ANSYS, Inc.*

[6] R.D. Williams, F.J. Keith and P.E. Allaire, Digital control of active magnetic bearings, *IEEE Transactions on Industrial Electronics*, **37**, 1990, pp. 19-27.

[7] COMSOL MULTIPHYSICS® Academic Research, Release 4.2b, *Structural Mechanics Module Analysis Guide, COMSOL, Inc.*

[8] S.W. Tsai. *Theory of Composites Design*. Think Composites. Dayton, USA, 1992.